BRAIN
ORIGINAL ARTICLE

Seizures initiate in zones of relative hyperexcitation in a zebrafish epilepsy model

James E. Niemeyer,[1,2] Poornima Gadamsetty,[1] Chanwoo Chun,[3] Sherika Sylvester,[3] Jacob P. Lucas,[1] Hongtao Ma,[1,2] Theodore H. Schwartz[1,2] and Emre R. F. Aksay[3]

Seizures are thought to arise from an imbalance of excitatory and inhibitory neuronal activity. While most classical studies suggest excessive excitatory neural activity plays a generative role, some recent findings challenge this view and instead argue that excessive activity in inhibitory neurons initiates seizures.
We investigated this question of imbalance in a zebrafish seizure model with two-photon imaging of excitatory and inhibitory neuronal activity throughout the brain using a nuclear-localized calcium sensor. We found that seizures consistently initiated in circumscribed zones of the midbrain before propagating to other brain regions. Excitatory neurons were both more prevalent and more likely to be recruited than inhibitory neurons in initiation as compared with propagation zones. These findings support a mechanistic picture whereby seizures initiate in a region of hyperexcitation, then propagate more broadly once inhibitory restraint in the surround is overcome.

1 Department of Neurological Surgery, Weill Cornell Medicine, New York, NY 10065, USA
2 Feil Family Brain and Mind Research Institute, Weill Cornell Medicine, New York, NY 10065, USA
3 Institute for Computational Biomedicine and the Department of Physiology and Biophysics, Weill Cornell Medicine, New York, NY 10065, USA

Correspondence to: Hongtao Ma, PhD
Department of Neurological Surgery
Weill Cornell Medicine
New York, NY 10065, USA
E-mail: hom2001@med.cornell.edu

Correspondence may also be addressed to: Theodore H. Schwartz, MD
Department of Neurological Surgery
Weill Cornell Medicine
New York, NY 10065, USA
E-mail: schwarh@med.cornell.edu

Keywords: *E/I* balance; seizure propagation; seizure initiation; calcium imaging; ictogenesis

Abbreviations: *E:I* = excitation:inhibition; FOV = field of view; LFP = local field potential; PTZ = pentylenetetrazol

Introduction

Excitation and inhibition are countervailing forces of brain activity that, in normal brains, operate in balance. However, in certain pathological brain states, such as epileptic seizures, this excitation:inhibition (*E:I*) balance goes awry. While traditional doctrine held that seizures resulted from hyperactive excitatory drive,[1–4] recent studies in various models have suggested a generative role for inhibitory neuronal subtypes in ictal onset. This revised picture has been supported by observations of increased inhibitory activity in pre-seizure periods.[5–8] For example, low-voltage fast seizures in humans are marked by early inhibitory cell firing prior to peak excitatory cell activity.[7] Evidence for a direct causal role of inhibitory cells in seizure onset is also reported.[9–11] For example, blocking the effects of inhibitory activity with a GABA antagonist (picrotoxin) can paradoxically prevent spontaneous seizures in a genetic mouse model of human autosomal-

Received June 02, 2021. Revised February 03, 2022. Accepted February 05, 2022. Advance access publication February 23, 2022
© The Author(s) 2022. Published by Oxford University Press on behalf of the Guarantors of Brain. All rights reserved. For permissions, please e-mail: journals.permissions@oup.com

dominant frontal lobe epilepsy.[9] Another study showed that optogenetic stimulation of specific interneuron subtypes (parvalbumin- or somatostatin-positive cells) can initiate seizures.[11] Together, these finding challenge the traditional concept of excitatory neuron hyperactivity as the primary driver of seizure initiation.

However, the role of inhibitory cells in seizure onset is still widely debated. Not only are there data showing that inhibitory cell activation can inhibit seizure onset,[12] but activation of inhibitory cells has been clearly shown to shorten seizure duration.[13,14] While differences in seizure models, experimental preparations and recording techniques could explain these disparate results, the explanations may be more subtle. While one recent study found that inhibitory cells can exert either anti- or pro-seizure effects depending on the timing of activation,[15] another showed that the effects of excitatory and inhibitory cells may be spatially dependent.[16] These findings suggest that the role of *E*:*I* balance in seizures may not be as simple as 'more *E*' or 'earlier *I*', but rather that the effects of *E*:*I* balance on ictal onset and evolution may be spatiotemporally contingent.

Understanding how *E*:*I* balance plays into ictogenesis has several experimental requirements. First, a large region of brain, inclusive of various interconnected structures, must be analysed during seizure periods. Ideally, this areal sampling would include both the site of seizure initiation as well as sites of later seizure propagation. Second, the neural activity analysed should simultaneously include both *E* and *I* information that can be separated with single-cell resolution. Finally, the neural activity should be recorded in awake animals whose activity can best recapitulate seizures lacking the confounding effects of anaesthesia.

These criteria can be relatively easily met in the zebrafish preparation.[17] These vertebrates exhibit significant homology with humans at the genetic,[18] neurochemical and brain structural[19] levels. Their transparency, rapid development and small size in the first few weeks after fertilization allows whole-brain optical access at subcellular resolution. Their genetic tractability permits tissue and cell-type specific experimentation. Further, their ease of handling facilitates both high-throughput drug screening[20,21] and high-resolution imaging and electrophysiological studies in the unanaesthetized animal. Prior work on seizures using this animal model has already shown similar electrographic profiles,[22] glial involvement[23] and responses to seizure treatments[24] as found in human epilepsy.

Here we used the zebrafish model to investigate spatiotemporal variations in *E*:*I* balance during seizure initiation and propagation. We monitored seizure dynamics using both electrophysiological recording and two-photon calcium imaging that enabled tracking of neuronal dynamics across the brain at the single cell level. We found specific regions of the brain consistently associated with seizure initiation, while others with seizure propagation. Using transgenic specification to separate excitatory and putative inhibitory populations, we found that the ratio of *E*:*I* activation at ictal onset was greatest in initiation zones. This finding demonstrates the importance of early excitation at triggering ictal events in the zebrafish model and challenges recent reports arguing that early inhibitory neuron activity is the key driver in initiating seizures.

Materials and methods

All experiments were performed in accordance with the guidelines and approval of Weill Cornell Medicine's Institutional Animal Care and Use Committee. Further methods details, including descriptions of algorithms used, can be found in the Supplementary material.

Zebrafish preparation

Mutant zebrafish larvae [*Tg(HuC:h2b-GCaMP6f)* × *Tg(Vglut2a:dsRed)*][25–27] were used at 5–8 days after fertilization—the h2b-tag localizes GCaMP to the nucleus to disambiguate the site of origin of the signal by eliminating contamination from axonal and dendritic sources. Larvae were embedded in agarose and then the electrode was inserted (see below). The larva was then paralysed by pancuronium bromide (Sigma P1918-10MG) and covered in Evans medium. Epileptiform activity was induced by bath application of 15 mM pentylenetetrazol (PTZ; Sigma P6500-50G), which is more commonly used and effective than alternatives such as pilocarpine[23] and 4-aminopyridine.[28]

Electrophysiology

During calcium imaging, the local field potential (LFP) was recorded using a glass microcapillary to avoid obstructing fluorescence excitation and light collection. Capillaries (1B120F-4, WPI) were pulled to a fine tip with vertical puller (P30, Sutter Instruments) to a tip diameter of 2–3 μm and filled with 4M NaCl after front-loading molten agarose (1.7% Ultrapure Agarose, Thermo) to the tip to prevent diffusion of the electrode solution once inserted into the brain. When tested in Evans medium, these electrodes had a resistance of 1–3 MΩ. The electrode was inserted through an incision in the skin into the neuropil of the right optic tectum. Recordings were made with a microelectrode amplifier (Model 1800, A-M Systems) using bandpass filtering (between 0.1 and 1 kHz) at 10-kHz sampling rate and digitized using custom MATLAB code.

Two-photon imaging

A custom-built two-photon microscope was used for imaging calcium activity and fluorescence in the embedded zebrafish. A MaiTai HP laser (Newport) was used to focus a 915-nm pulsed light beam through a water immersion 40×/0.8 NA objective (OBJ1; LUMPlanFl40XW/IR2, Olympus) onto the fish. Multiple separate horizontal planes of the fish were acquired sequentially in the dark. Across all animals our imaging depth ranged 120–230 μm from the surface (measured at the bisector of the midbrain–hindbrain border); we imaged about 3–5 planes within this range in each animal, with spacing typically ∼30 μm between planes. At each plane, imaging was performed at 2 Hz (256 × 256 pixels, 550 × 550 μm), providing different fields of view (FOVs) from the same fish. The emitted light from the zebrafish larva was collected by the objective and directed towards two dichroic mirrors (DM1, 720dcxruv; DM2, 565dcxr; Chroma Technology), which reflected this light into two separate channels of green (F3; ET525\50m-2p; Chroma) and red (F2; ET605 \70m-2p, Chroma) to then be amplified by the photomultiplier tubes (R3896, Hamamatsu). A substage photodetector (PDA36A, Thorlabs) detected light scattered from the focal plane and together with signal from the photomultiplier tubes was processed by MATLAB-based software ScanImage[29] to generate fluorescence images.

Electrophysiology

Electrographic data were used to validate and examine ictal events during two-photon imaging. The spectrogram of the LFP was calculated using short-time Fourier transform ('spectrogram' in MATLAB), with a window width of 0.1 s. Time of onset in the

epileptiform events was determined using a statistical method based on the mean and 3 standard deviations (SD) of the power between 1 and 60 Hz during a 5-s interictal window. For electrographic analyses (Fig. 1 and Supplementary Fig. 1), the first increase in power > 3 SD above the baseline was established as the onset of an event (interictal or ictal). The termination was set at the moment the LFP power returned within 3 SD of baseline.

Image analysis

Pre-processing

Imaging data files were de-interleaved in Fiji[30] to extract the green (GCaMP6f) and red (DsRed) channels. Rigid motion correction was applied in MATLAB 2018a using the NoRMCorre algorithm and toolbox[31] on the red channel images, which did not contain activity-dependent fluorescence, and then the correction was applied to the green GCaMP channel as well. We used these data sets to examine ictal event activity across brain regions with two overarching analysis methods: (i) pixel-wise methods to characterize ictal event initiation and propagation; and (ii) single-cell analyses to examine differences in VGlut2+ excitatory neurons and putative inhibitory interneurons during seizures.

Correlation coefficient masks

During ictal events, GCaMP6f fluorescence in the image increases as the ictal event initiates and propagates through the brain. To create a mask identifying the extent of the brain that is involved in seizure events, we first de-noised the data by applying a two-dimensional Gaussian filter ($\sigma = 2$ pixels, ~4 µm) and then smoothed individual pixels over time (Butterworth, first order, cut-off frequency of 0.2 Hz). We then correlated each pixel time series to that of whole-brain activity and selected those pixels where Pearson's correlation exceeded 0.6.

Lag analyses for individual ictal events

Global ictal events were identified as those where the peak of the spatially averaged calcium fluorescence event exceeded 2 SD above the mean of the time series average (see 'Results' section, Fig. 1D, for association between global calcium signal and ictal electrophysiological signatures). We chose to use an optical

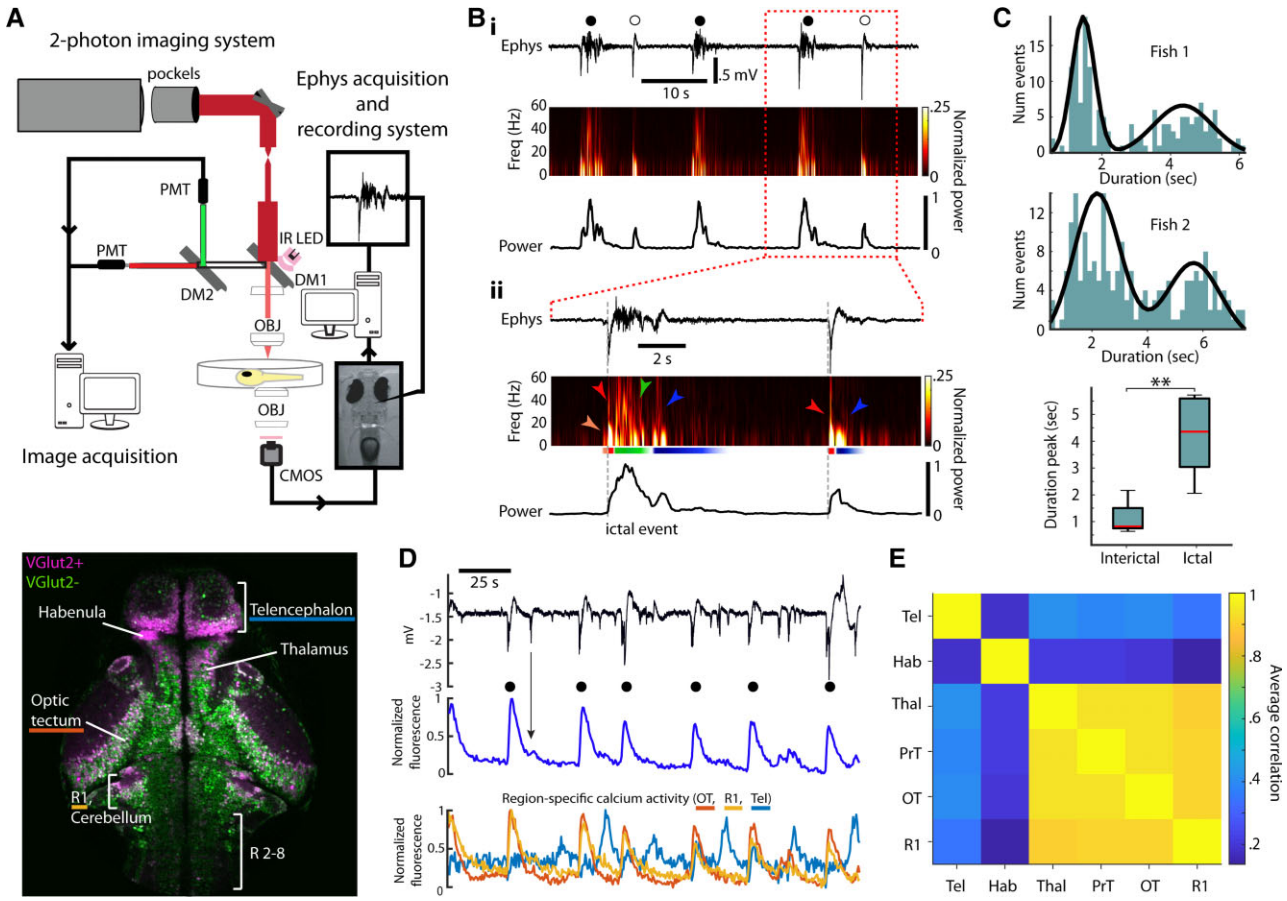

Figure 1 Ictal and interictal activity in the larval zebrafish. (**A**) *Top*: Experimental setup for two-photon imaging and electrophysiology in larval zebrafish during seizures. *Bottom*: Single imaging plane revealing distribution of VGlut2+ (magenta) and VGlut2– (green) cells in a variety of brain regions (R = rhombomere). (**B**) Electrophysiological signatures of ictal- and interictal-like events in the zebrafish. (i) *Top*: LFP; *middle*: spectrogram; *bottom*: total power during a period of ictal (filled circle) and interictal (open circle) events. (ii) Similar organization as above but at finer time resolution, with indication of distinct sections (orange, red, green, blue) characterizing the time-course of the two types of events. (**C**) *Top*, *middle*: Histograms of event duration times for two fish and best fit (black) with a Gaussian mixture model; *bottom*: for all fish, duration time for ictal and interictal events. (**D**) *Top*: LFP; *middle*: globally averaged change in GCaMP6f fluorescence; *bottom*: regional change in fluorescence during a series of ictal (filled circle) and interictal events (OT = optic tectum; R1 = rhombomere 1; Tel = telencephalon). (**E**) Matrix of correlations in the activity among various brain regions (Hab = habenula, Thal = thalamus, PrT = pretectum).

measure for defining global ictal events because electrophysiological recordings, on occasion, developed noise that obscured our ability to cleanly identify these events (possibly due to tissue obstruction of the tip). All individual ictal events were verified by visual examination.

We then visualized the relative timing of seizure onset at different brain regions. This was done by first identifying the peak first derivative of global activity, yielding the time at which the ictal event was increasing most rapidly in the fluorescence data. We then created a global template of whole-image ictal event activity that ended at this point and began 6 s prior to this point. This template was compared with individual pixel activity to find the time of maximum correlation, yielding a matrix of the times when each pixel was significantly recruited to the ictal event. When visualized as a heat map, this matrix provides a 'lag map' where the ictal event activity began and spread across the imaging field of view. A total of 10 separate animals produced $n = 174$ ictal events. We then used MATLAB's edge detection functions to extract the regions where ictal initiation occurred in the earliest 500 ms, eliminating false positives by requiring at least 300 connected pixels (~0.5% of the 256 × 256 images). We labelled these sites 'initiation sites' and labelled zones which activated later 'propagation sites'.

Single-cell analysis

We extracted cells from the unsmoothed GCaMP6f images using a semi-automated MATLAB algorithm. We excluded any neurons not at least $r = 0.3$ correlated with the average activity of all extracted cells. On average, we extracted 351 seizure-active cells per FOV. To separate putative inhibitory (expressing only GCaMP) and excitatory cell types (coexpressing DsRed and GCaMP in VGlut2+ cells) we examined the red intensity values from individual cells and used a Gaussian mixture model to define cell identity based on the bimodal distribution of red intensity (noise versus DsRed). In two data sets we could not confidently extract *E* versus *I* cell type differences; therefore, the seven ictal events in those data series were not included in our *E*:*I* single-cell analyses leaving $n = 167$ ictal events.

Seizure onsets

Single-cell involvement in seizures was determined by identifying the times at which individual cells became significantly involved in the ictal events. We compared single-cell activity traces with a new global response template (see Supplementary material), centring the template on the peak second derivative, a time that more accurately represents true ictal event onset compared to other methods of cut-offs such as half-height or 2 SD above the mean. The single-cell onset was defined as the time of highest correlation between these traces in a sliding window (Supplementary Fig. 4). When temporally aligning data, we used the average ictal onset time calculated across all cells significantly recruited to each individual seizure, a procedure analogous to the relative times calculated in our lag analyses above. Thus, data are displayed relative to this time-zero point.

Excitation:inhibition (*E*:*I*) balance

We examined *E*:*I* relationships by calculating an *E*:*I* ratio index. We use this method instead of simple *E*/*I* ratio because in some cases we observed low numbers of cells in our initiation sites. *E*:*I* index values in initiation regions were calculated by summing these cell types within the earliest active brain areas (see above, Lag analyses). *E*:*I* ratios in propagation zones were calculated the same way, using remaining areas of the brain that were significantly involved in seizures (propagation zones). The index value was calculated as

$$EI_{\text{index}} = \frac{E - I}{E + I}, \tag{1}$$

where *E* and *I* are counts of *E* and *I* cells. The *E*:*I* ratio index provides a measure of the relative differences in amounts of *E* and *I* cells located in the initiation and propagation regions. Note that when comparing the *E*:*I* index values (or any *E*:*I* measure) between two brain regions, there are multiple scenarios that can lead to relative differences in these indexes. For example, if one observes a higher *E*:*I* index in initiation zones relative to propagation zones, this could have been due to an increase in *E* or a decrease in *I* at the initiation site, but also due to a decrease in *E* or an increase in *I* at the propagation site.

We measured excitatory and inhibitory cell recruitment throughout ictal events by temporally aligning all events and then calculating the fraction of *E* and *I* cells significantly involved in the ictal events before and after the onset.

Ictal versus interictal brain state and network analyses

Dimensionality metric

A population of *N* neurons makes an activity trajectory in the *N* dimensional space over some time points (*T*). The effective dimensionality of the trajectory can be quantified with the uniformity of the singular values (λ_i) of the trajectory matrix (*N* by *T*, mean-subtracted).

$$q = \frac{\left(\sum_{i=1}^{\min(N,T)} \lambda_i\right)^2}{\sum_{i=1}^{\min(N,T)} \lambda_i^2} \tag{2}$$

If the singular values are perfectly uniform, all principal components explain equal amount of variance, and therefore the effective dimensionality should maximal. If only one singular value is non-zero, then the effective dimensionality should be 1. For our dimensionality analysis, the number of cells (*N*) was variable but always greater than the number of time points ($T = 10\text{ s} \times 2\text{ Hz} = 20$ samples) of our time window, so the upper limit of the dimensionality was fixed at *T*. This allowed us to compare the effective dimensionality across trials with different number of cells without further adjustments. A dimensionality at an instantaneous time point *t* is estimated by calculating the dimensionality over the time window centred around *t*. The instantaneous estimation was used to construct a time series from which we could visualize the time evolution of dimensionality.

Excitatory and inhibitory correlations

Populations of excitatory cell pairs and inhibitory cell pairs were analysed for their correlations around ictal events. The correlation metric (*C*) is an average pair-wise correlation value of the calcium traces over a time window (1.5 s),

$$C_{J,K} = \frac{1}{|J||K|} \sum_{j \in J} \sum_{k \in K} corr(X)_{j,k}, \tag{3}$$

where X is a matrix whose rows are a time series of a single cell within the rolling time window and J and K are sets of indices for excitatory or inhibitory cells. $corr(X)$ returns a correlation matrix. Self-correlations (diagonal elements) are ignored. A correlation at an instantaneous time point t is estimated by calculating the correlation over the time window centred around t. The instantaneous estimation was used to construct a time series from which we could visualize the time evolution of correlation.

Data availability

Motion-corrected data gathered in this work is available at the following: Niemeyer, James, Gadamsetty, Poornima, Chun, Chanwoo, Sylvester, Sherika, Lucas, Jacob, Ma, Hongtao, Schwartz, Theodore, & Aksay, Emre. (2022). Zebrafish 2-photon imaging data during seizures; Original data [Data set]. Zenodo. https://doi.org/10.5281/zenodo.5931656.

Results

We present our investigation of the spatiotemporal dynamics of *E*:*I* balance during seizures as follows. First, we introduce the experimental preparation and describe electrophysiological characterization of interictal and ictal events in this epilepsy model (Fig. 1). Next, we present a pixel-based timing analysis (Fig. 2) that is used to create maps of the spatiotemporal dynamics in the brain during seizures (Fig. 3). We then examine timing at a cellular level in excitatory and inhibitory populations in regions designated as 'initiation' and 'propagation' zones (Fig. 4). Finally, we confirm that findings from our single-cell analysis hold at the network level (Fig. 5) and when examined with spatial specificity using correlation analysis (Fig. 6).

Experimental paradigm for examining excitation and inhibition

Experiments were performed using larval zebrafish with all neurons expressing GCaMP6f and VGlut2+ cells expressing DsRed (Fig. 1A). The first fluorophore, h2b-tethered GCaMP6f, is a fast calcium sensor that is localized to the nucleus to eliminate contamination from neuropil signal and enable better separation of signals between cells.[26] The second fluorophore, DsRed, was used to help separate excitatory from inhibitory neurons. VGlut2 is a vesicular glutamate transporter gene found in the vast majority of glutamatergic cells in the larval zebrafish.[25] The largest proportion of VGlut2– cells are inhibitory GABAergic neurons, with non-trivial contribution from excitatory VGlut1 cells (primarily cerebellar granule neurons) and inhibitory glycinergic neurons. Due to the purely excitatory nature of the VGlut2+ population and the primarily inhibitory nature of the VGlut2– populations, below we refer to the former as 'excitatory (*E*)' neurons and the latter as 'inhibitory (*I*)' neurons.

Seizure characterization by electrophysiology and calcium imaging

Our first goal was to characterize seizures measured electrographically. Seizures were induced using bath-applied PTZ in larval zebrafish that were held in agar. While the definition of a 'seizure' can be flexible and the exact features of seizures likely vary between species and models, our electrophysiology data below demonstrate separable ictal-like and interictal-like events with electrographic signatures similar to those observed in other animal models and humans. For simplicity, here we use the word 'seizure' to refer to the ictal events as others have done for PTZ-induced ictal activity in zebrafish.[23,28,32] In initial two-electrode experiments, we placed electrodes in different brain regions (telencephalon, optic tectum, or hindbrain) and found that ictal events developed concurrently after ~15 min of PTZ application. Electrodes placed in the optic tectum consistently captured the largest set of ictal events (unpublished observations)—hence, in subsequent experiments, we used only one electrode placed in the neuropil of the optic tectum. Fig. 1B(i) shows an example electrophysiology recording, demonstrating ictal-like events lasting for several seconds ('ictal', filled circle symbol), followed by quiescent periods and occasional brief interictal-like events ('interictal', open symbol), as well as their corresponding power spectrograms. Ictal events [Fig. 1B(ii), left] were marked by an initial low-frequency power increase (orange), a brief cross-frequency spike with most power <20 Hz (red), a sustained phase with a more uniform cross-frequency distribution (often up to 100 Hz) that lasted for several seconds (green), and a recovery phase at lower frequency with gradual relaxation (blue). In contrast, interictal events (right) only exhibited the short cross-frequency event (red) before moving to a briefer recovery phase than seen with ictal events (blue). Examining the histograms of event durations revealed a bimodal distribution where those events with the strongest ictal features exhibited durations that were on average a factor of 4 greater than those events with predominantly interictal features (Fig. 1C; Wilcoxon signed-rank test, $n = 9$ fish, 1685 events, $P = 0.003$).

We next employed simultaneous cellular-resolution two-photon imaging of larval zebrafish along with the electrophysiological recordings. Ictal events identified electrographically were associated with large fluorescence increases globally averaged across the field of view spanning the brain (Fig. 1D, black circles; Supplementary Fig. 1). Interestingly, most ictal events involved coordinated calcium signalling across the mid- and hindbrain, with the forebrain either not involved or asynchronously activated (Fig. 1D bottom; Fig. 1E, $n = 5$ fish, 22 seizures). Interictal events, on the other hand, did not lead to significant changes in globally averaged activity (Fig. 1D, for example see black arrow). This clear association between electrophysiologically identified ictal activity and strong global fluorescence was present regardless of our imaging depth (data not shown).

Lag maps identify regions of seizure initiation and illustrate seizure propagation

To examine the involvement and timing of different brain areas in PTZ seizures we next developed a method to extract seizure propagation maps within individual fish. We first used correlation to global average ictal activity to create a mask that excluded pixels where there were no changes in fluorescence related to the seizure (Fig. 2A). The activity in the retained pixels was not monolithic, with some regions beginning to show elevations in fluorescence well before other regions (Fig. 2B, red arrows). To examine these temporal variations more carefully, we correlated pixel-level activity to that of a template of ictal activity initiation defined from a segment of the global fluorescence event (Fig. 2C, middle), generating a propagation map for each ictal event by incrementally shifting the template in time to identify when activity in a particular pixel began to rise (see 'Methods'; Fig. 2C, right). This template-matching procedure allowed identification of the earliest portions of the ictal activity in each pixel and was less susceptible to errors than

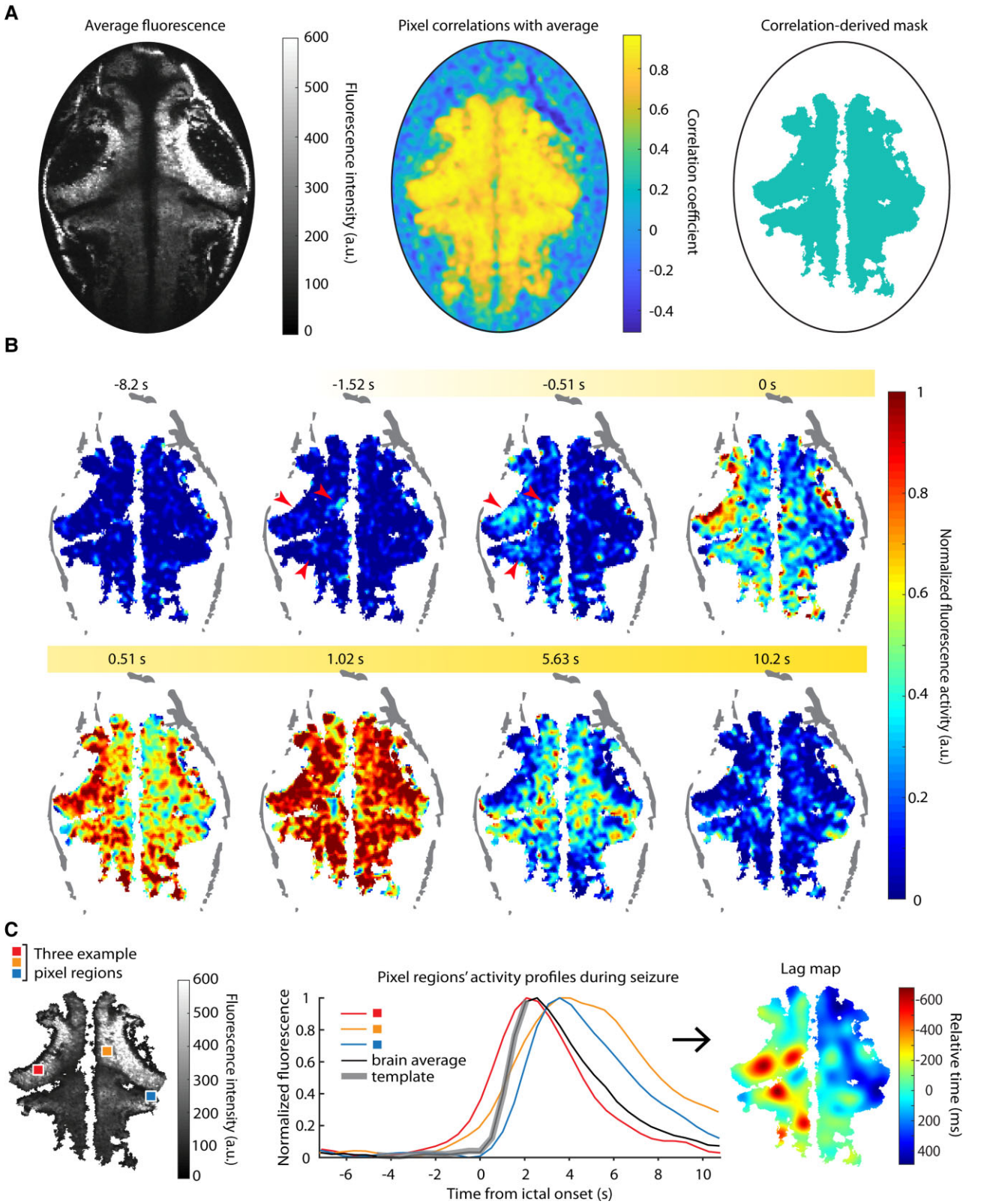

Figure 2 Ictal event mapping. (**A**) *Left*: Average fluorescence over a series of ictal events in one brain; *middle*: pixel-wise correlation with brain average; *right*: the correlation mask. (**B**) A single seizure's fluorescence activity is shown over time; red arrows highlight early activity. (**C**) *Left*: Sample pixels and their activity profiles (*middle*) over a single seizure are shown; *right*: the corresponding smoothed lag map for this seizure shows the relative activation times for each pixel with respect to the brain average.

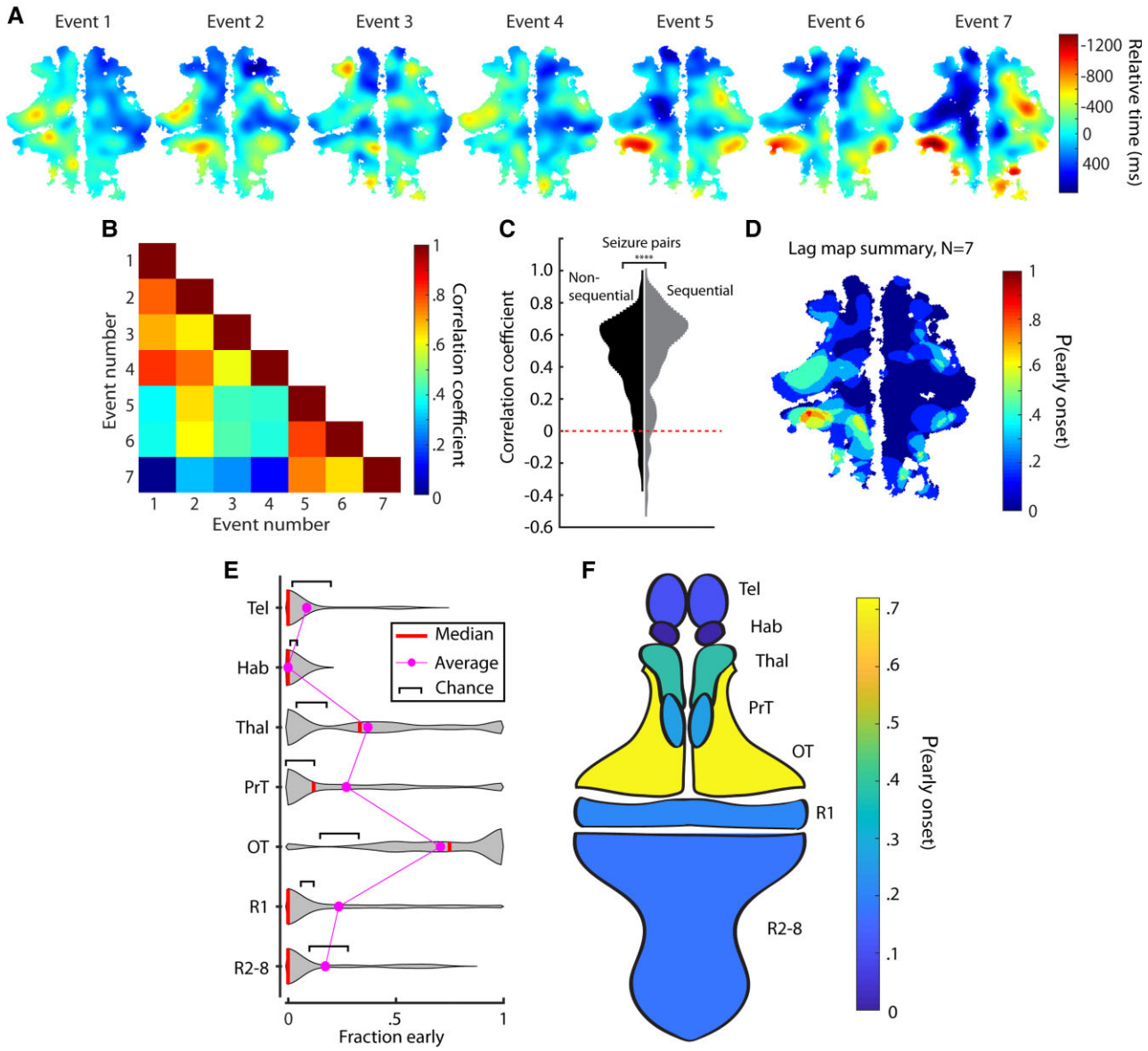

Figure 3 Ictal events evolve similarly within fish but initiate in different regions across fish. (**A**) Lag maps for seven seizures in one animal. (**B**) Correlations between the events in **A**. (**C**) Correlations of all pairs of sequential and non-sequential ictal events recorded. (**D**) Summary map of the ictal events in **A**. Violin plots (**E**) and a schematic fish brain map (**F**) of early-onset regions show where ictal events initiated most commonly across different fish.

procedures that relied upon threshold crossings or features such as peak fluorescence.

We applied this algorithm to create a lag map for each individual ictal event ($n = 10$ fish, $n = 174$ ictal events). Fig. 3A shows the lag maps of seven ictal events in one larval zebrafish (the same animal as Fig. 2). This revealed a similarity between neighbouring ictal events (e.g. Events 1–4 versus 5–7). In this animal the left cerebellum and the optic tectum showed consistent early involvement in every ictal event. To quantify how similar ictal propagation appeared between ictal events, we measured the correlation coefficient of the 2D spatiotemporal lag maps of all pairs of ictal events for this animal (Fig. 3B). This similarity was quantified for the entire data set by pooling within-animal correlations, revealing a positively skewed distribution (Fig. 3C). Interestingly, when we separated seizure pairs into sequential (seizures happening next to each other in time) and non-sequential, we found significantly more similarity for the temporally adjacent seizures compared with the other seizure pairs (Fig. 3C, Wilcoxon rank sum test $P < 0.0001$, $n = 803$ non-sequential seizure correlations, $n = 151$ sequential seizure correlations).

We next developed a scheme to summarize these spatiotemporal patterns and identify regions consistently involved in seizure initiation. Lag maps for individual ictal events were binarized by assigning a value of 1 to all pixels where neuronal activity initiated at least 500 ms in advance of the population event and a value of 0 to all other pixels. Averaging these mask arrays across all events within a single fish provided a two-dimensional summary showing where ictal events initiated most frequently for that animal (Fig. 3D). For the animal whose seizures are displayed in Fig. 3A, we see that the left cerebellum and portions of the left tectum exhibit the highest

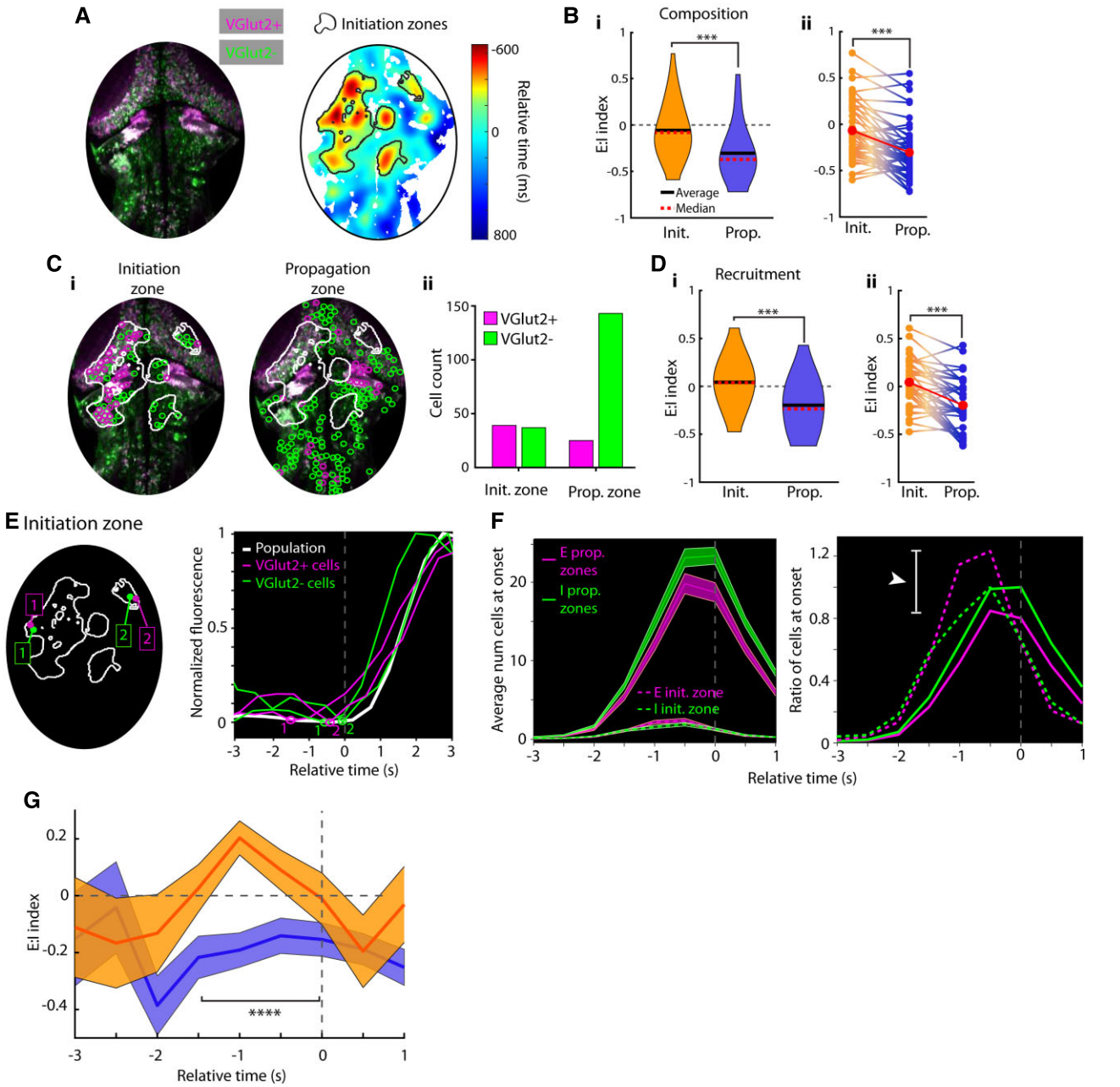

Figure 4 Greater prevalence and recruitment of excitatory neurons in ictal initiation zones. (**A**) A sample fish image with *E* and *I* cells differentially labelled and its associated lag map and initiation zone for a single ictal event analysed in this figure. (**B**) *E*:*I* index in initiation and propagation zones (**i**) and within-seizure *E*:*I* comparisons (**ii**). (**C**) Single cell locations in a seizure, split by initiation versus propagation zone location (**i**) and cell counts from initiation and propagation zones (**ii**). (**D**) *E*:*I* index of cells recruited to seizures in initiation and propagation zones (**i**) and within-seizure *E*:*I* index comparisons (**ii**). (**E**) *Left*: Sample excitatory and inhibitory cells from initiation zones; *right*: their associated calcium traces during this event. Detected onset times are plotted on traces. (**F**) *Left*: Average number of cells at onset across all ictal events grouped by initiation or propagation zone membership; *right*: the ratio of cells at onset (*E*:*I*) over time, normalized to by the number of inhibitory cells at onset. (**G**) *E*:*I* ratio index calculated in initiation (orange) and propagation (blue) zones. All error bars are mean ± SEM.

probability of involvement in ictal initiation. Across all animals ($n = 10$), the most common initiation zones were the optic tectum, thalamus, pretectum and cerebellum/R1 (Fig. 3E and F). Across FOVs we used the area (μm^2) of individual regions as a fraction of the overall brain to measure the probability of a seizure initiating in one region if initiation sites were based on chance (shown as black brackets, Fig. 3E). We found that the average and median frequencies of seizure initiation in thalamus and optic tectum were both significantly higher than chance (Wilcoxon rank sum test, $^{*}P < 0.05$, $^{***}P < 0.001$; thalamus: initiations $n = 32$, FOVs $n = 25$. Optic tectum: initiations $n = 33$, FOVs $n = 26$). For rhombomere 1 and the pretectum, the average fraction early was above chance, although by median comparison these regions were not significantly above chance (Wilcoxon rank sum test, $P > 0.05$; rhombomere 1: initiations $n = 29$, FOVs $n = 20$. Pretectum: initiations $n = 30$, FOVs $n = 25$). Meanwhile, the telencephalon, habenula, and rhombomeres 2–8 all showed

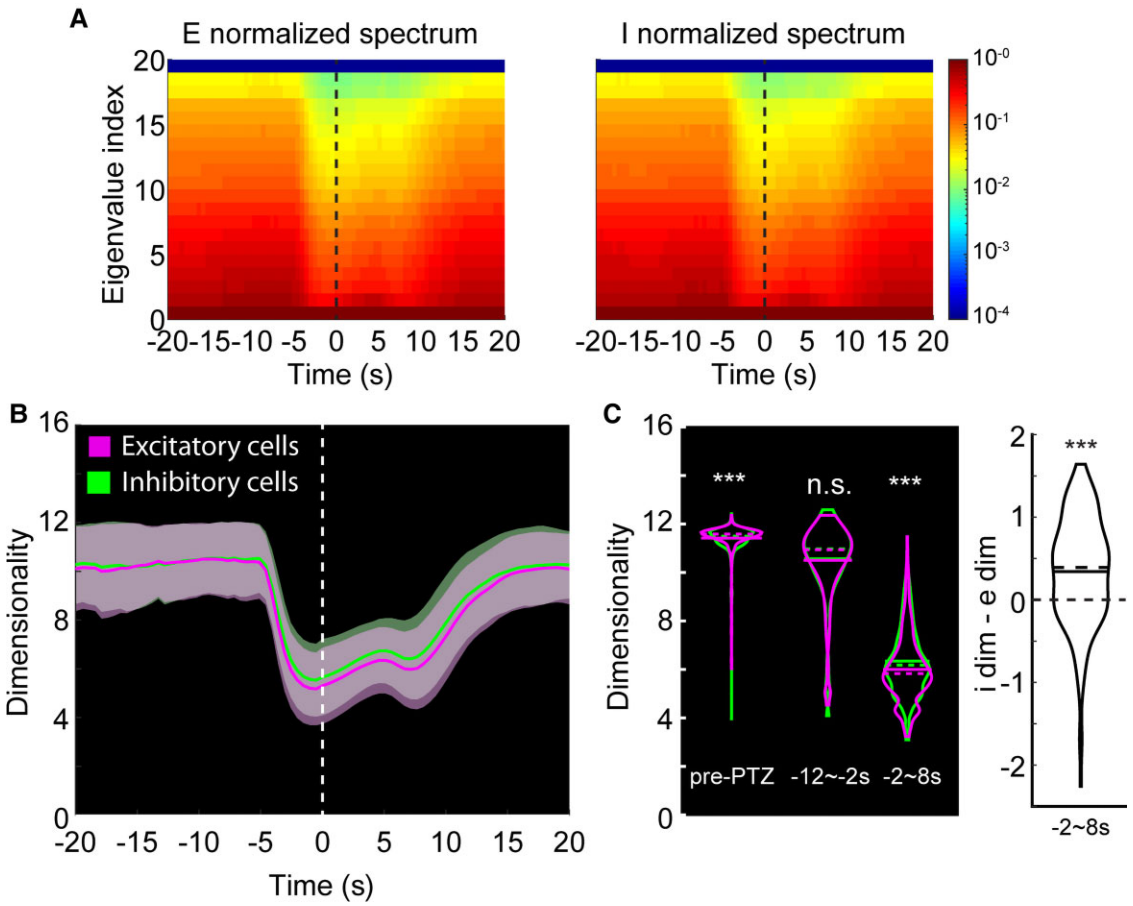

Figure 5 Dimensionality of the excitatory and inhibitory cell population activities. (**A**) *Left*: Eigenspectrum of the excitatory population activity over 10 s-wide rolling window, normalized to the greatest eigenvalue per time point. Vertical line at time 0 is the ictal onset point. *Right*: Same analysis done for inhibitory cell population. (**B**) Average trends of the dimensionality. Vertical line at time 0 is the average ictal onset point. Dimensionality over 10-s moving window [magenta: excitatory cell pairs (*e*-*e*); green: inhibitory cell pairs (*i*-*i*)]. (**C**) *Left*: Dimensionalities of *i*-*i* pairs and *e*-*e* pairs shown separately for pre-PTZ, −12∼−2 s and −2∼8 s periods relative to the average ictal onset point. *Right*: Differences in *I*-*E* dimensionalities at −2∼8 s.

average and median initiation frequencies that occurred at or below chance (Wilcoxon rank sum, $P > 0.05$, telencephalon: initiations $n = 24$, FOVs = 23; habenula: initiations $n = 15$, FOVs $n = 15$; rhombomeres 2–8: initiations $n = 20$, FOVs $n = 20$). Propagation zones were defined as the remainder of the brain to which the seizure spread outside the initiation zone.

Excitation and inhibition examined in seizure initiation and propagation zones

Having identified the ictal initiation and propagation zones, we next focused on the issue of *E*:*I* balance in these different regions during seizures. We first asked if there were differences between the initiation and propagation zones in the relative numbers of excitatory and inhibitory cells. Taking advantage of the ease with which single neurons can be distinguished with nuclear-localized GCaMP6f, we labelled individual soma using standard computer vision algorithms and separated them into excitatory and inhibitory cells based on the intensity of the DsRed fluorophore (total $n = 19\,434$ cells across nine fish; example event and seizure-recruited cells shown in Fig. 4A). An event-specific comparison of the differences between the initiation and propagation regions in composition was performed by calculating, for each ictal event, a value for an *E*:*I* composition index; the index was defined such that a region with only excitatory cells had a composition index value of 1, all inhibitory cells an index of −1, and an equal number of excitatory and inhibitory cells an index of 0. *E*:*I* composition in initiation regions was −0.07 ± 0.29 (SEM), while *E*:*I* composition in propagation regions was −0.30 ± 0.29 [Fig 4B(i); at cut-off requiring at least 10 *E* and 10 *I* cells per initiation site, $n = 49$ seizures]. Calculated over all animals and all seizures, this difference corresponds to a roughly 61% increase in the *E*:*I* ratio in the initiation zone relative to the propagation zone. This relative increase was also evident when composition values were compared on an individual event basis [Fig. 4B(ii), Wilcoxon signed-rank test $P < 0.001$]. This finding was robust to variation in the minimal number of cells of each type allowed in each region (Supplementary Fig. 3).

We next investigated if there were differences between the initiation and propagation zones in the relative numbers of excitatory and inhibitory cells that were recruited into the ictal event. Cells were deemed to be recruited into the seizure if they exhibited of correlation of 0.8 or better with the global ictal event (Supplementary Fig. 4). The locations of such cells during one seizure event are shown in Fig. 4C, revealing a much larger *E*:*I* ratio of recruited cells within the initiation zone than in the propagation zone. To quantify this observation across, we calculated an *E*:*I* recruitment index, defined as above but only for recruited cells. *E*:*I* recruitment in initiation regions was 0.04 ± 0.25 (SEM), while *E*:*I* recruitment in propagation regions

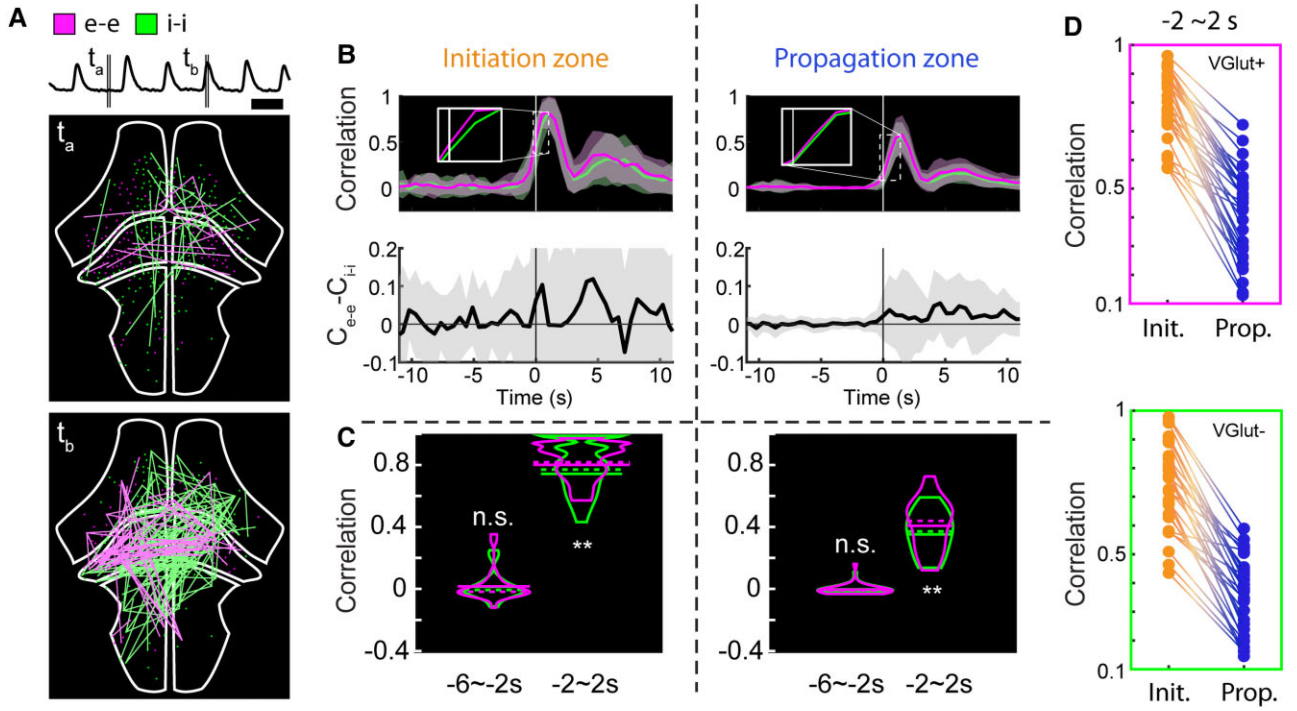

Figure 6 Excitatory and inhibitory cell network correlations. (**A**) Visualization of activity correlations at the cross-section of the whole brain. Only pairs with correlation values higher than 0.999 are shown. *Top*: Average normalized fluorescence trace. *Middle*: Correlations during interictal period. Magenta: Highly correlated excitatory cell pairs (*e-e*); green: inhibitory cell pairs (*i-i*). *Bottom*: Correlations during ictal period. Scale bar = 20 s. (**B**) Average trends of interictal to ictal transition for the initiation and propagation zones. *Top*: Correlation metric calculated over 1.5 s-wide rolling window (magenta: *e-e*; green: *i-i*). *Bottom*: Difference of *e-e* and *i-i* correlations. (**C**) Correlation metric values of *i-i* pairs and *e-e* pairs shown separately for −6∼−2 s and −2∼2 s periods relative to the average ictal onset point. (**D**) Within-seizure correlations of *e-e* cell pairs (*top*) and *i-i* cell pairs (*bottom*) between initiation and propagation zones.

was −0.20 ± 0.28, a significant difference [$P < .0001$, $n = 167$, Wilcoxon signed-rank test; Fig. 4D(i) at cut-off requiring 10 *E* and 10 *I* cells per initiation site; this finding was robust to variations in correlation coefficient required for cell onset detection, Supplementary Fig. 7]. This corresponds to a roughly 64% increase in *E*:*I* ratio in the initiation zone relative to the propagation zone across seizures and was robust across varying cut-offs of cell counts (Supplementary Fig. 3). As in the composition data above (Fig. 4B), the *E*:*I* index values were not always above 0 at the initiation site; however, they were significantly higher in initiation versus propagation zones [Fig. 4D(ii), Wilcoxon signed-rank test $P < 0.001$]. Thus, on average there is both a greater fraction of excitatory cells in initiation zones relative to propagation zones, and these excitatory cells are also recruited at a higher fraction within the initiation zone.

We next examined how *E*:*I* recruitment during the ictal event varied over time in the initiation and propagation zones. We observed asynchronous single-cell onsets during ictal events. As expected, across our data set we observed significantly earlier onsets in the initiation zones compared to propagation zones (Fig. 4E and F and Supplementary Fig. 3C). Interestingly, in the propagation region, the number of newly recruited excitatory cells was always less than the number of newly recruited inhibitory cells (Fig. 4F, left, solid lines, $n = 167$ seizures). In contrast, in the initiation zone, the number of newly recruited excitatory cells was comparable to the number of newly recruited inhibitory cells at the beginning and end of the ictal event but was notably higher at a time approximately 1 s ahead of the ictal onset. To see this difference more clearly, we normalized these recruitment curves to the peak of the number of newly recruited inhibitory cells (Fig. 4F, right), revealing (i) that the number of newly recruited cells peaked earlier in the initiation zone; and (ii) a difference of over 50% at peak in the ratios of newly activated excitatory versus inhibitory cells between the initiation and propagation sites (white arrow, Fig. 4F). Quantifying these observations using the *E*:*I* recruitment index introduced above, we see that significant differences in the pattern of recruitment between the initiation and propagation regions are present in the period −1.5 to 0 s before ictal onset ($n = 36$ seizures with at least 10 *E* and 10 *I* cells in initiation zone, Wilcoxon signed-rank test $P < 0.0001$, Fig. 4G).

Network-level analyses reaffirm a privileged role for excitation at seizure initiation sites

We next examined if this privileged position for excitatory neurons during the initiation of seizures was also apparent in higher-order relationships between excitatory and inhibitory cells. We began by using principal components analysis to look at the overall degree of coordination in excitatory versus inhibitory populations during the seizure initiation process. For both groups, the number of dimensions needed to explain population dynamics dropped dramatically at the time of ictal onset (Fig. 5A and B). This collapse to lower dimensionality, an indication of greater coordination within a population, was most pronounced for the excitatory population (Fig. 5C; pre-PTZ $n = 2781$, post-PTZ $n = 167$, right: *I*-*E* dimensionality differences, Wilcoxon signed-rank test, $^{***}P < 0.001$, $^{**}P < 0.01$, n.s. not significant).

To examine this increased coordination of *E* cells versus *I* cells with greater temporal specificity and regional context, we next analysed correlation structure within these cell types by calculating a correlation metric (C) in a rolling time window (Fig. 6A). We

focused on correlations between excitatory-excitatory and inhibitory-inhibitory cell pairs. Average correlation was generally low for both pairings during baseline conditions and inter-ictal periods (Fig. 6B, top). Correlation increased dramatically for both pairings around the time of ictal initiation, with correlation change in the initiation zone on average larger and more advanced in time than that in the propagation zone. We found that excitatory cell pair correlation was slightly elevated relative to inhibitory cell pair correlation during ictal onset in both regions (Fig. 6B, insets); this elevation was clearer when looking at the correlation difference, which was largest around the time of ictal onset in the initiation zone (Fig. 6B and C, Wilcoxon signed-rank test, $n = 36$ seizures with 10 *E* and 10 *I* cells in initiation zones, $^{***}P < 0.001$, $^{**}P < 0.01$, n.s. not significant; Fig. 6D, within-seizure correlation differences in initiation and propagation sites in events with 10 *E* and 10 *I* cells). Thus, these correlation patterns further suggest that the coordinated activation of excitatory neurons in the initiation zone plays an important role in triggering ictal events.

Discussion

In this study, we addressed the question of *E*:*I* balance in seizure initiation and propagation using the zebrafish model. The main technical limitation afflicting prior studies of this topic has generally been the need for broad, cell-specific sampling of the widespread neuronal substrate inclusive of the ictal onset zone and all areas of potential propagation. We overcame these challenges using a global imaging strategy in the larval zebrafish, an optically transparent vertebrate preparation allowing for simultaneous imaging of multiple cell types. We demonstrated a privileged role for excitation over inhibition in the seizure initiation zone, while regions that were invaded later were biased towards stronger inhibitory cell recruitment.

Seizure dynamics in the larval zebrafish

These findings will aid efforts to identify seizure medications with high-throughput screening. Zebrafish are increasingly used to test potential drug treatments for neurological diseases such as epilepsy.[24,33] High-throughput drug screening is a primary method of therapeutic discovery,[34] and the zebrafish offers significant advantages in this regard due to the ease with which drugs can be delivered uniformly to the brain while behavioural changes are monitored *en masse*. However, while such high-throughput studies can be quite useful in identifying promising classes of drugs, optimization of both the therapeutic and its dosing will benefit greatly from a mechanistic understanding of the pathophysiology being addressed. The larval zebrafish affords several advantages for understanding the cellular and circuit mechanisms of the brain, including high-resolution optical access globally, a suite of genetic tools for monitoring and manipulating specific cell types, and the capacity to study all constitutive elements of an intact circuit. Here we have harnessed some of this power to begin understanding the pathophysiology of seizures. The preponderance of excitatory activity in the initiation zone points towards exploiting this model to screen, with greater granularity, classes of drugs that can preferentially regulate the activity of glutamatergic neurons in midbrain structures.

We triggered seizure events in the zebrafish model using PTZ, a chemoconvulsant commonly used in therapeutic screening. PTZ is the only pharmacological seizure-inducing drug employed at the initial identification stage by the NINDS Epilepsy Therapy Screening Program.[35] PTZ is known to induce seizures in humans[36,37] and lower seizure threshold in epileptic patients.[38] PTZ-induced seizures in the zebrafish occurred spontaneously, repeatedly and throughout the brain, consistent with earlier reports.[23,28,39,40] Furthermore, the ictal LFP showed spectral features[41] similar to those observed in rodent models[42] and human patients[43]: at initiation, ictal events displayed an abrupt broad-frequency power increase, followed by a longer period where power was restricted to a slightly lower frequency range, concluding with a return to baseline power at the time of termination. This commonality supports the idea that the PTZ model of ictogenesis in the zebrafish is of general relevance for the study of seizures in other species.

Spatiotemporal consistency of seizure initiation and propagation

Regions of ictal onset and propagation were generally conserved within fish, but somewhat varied between animals. Rodent slice experiments have shown that the seizure foci can change slowly over time: one focus can dominate for several minutes before being replaced by another region.[44] However, such studies have also found that certain brain regions (e.g. hippocampal CA2-3) and cell layers (neocortical layer 5 pyramidal cells) are predisposed to act as pacemakers in seizure-generating activity.[45,46] Our findings extend these results to an awake, whole-brain model. We found a significant level of consistency in initiation and propagation patterns within fish, although correlations weakened over tens of minutes. While there was some variation between animals, we found that midbrain structures had a quite high propensity to serve as initiation zones. We also confirmed the surprising finding that the telencephalon (homologous with human cortex) was one of the last regions to be recruited in the seizing zebrafish brain.[23] Thus, our results provide evidence that certain subcortical sites may serve a prominent role in generalized seizure initiation,[47–53] although these results do not negate a role for cortical contributions.

E:*I* balance differs in initiation and propagation zones

Synchronous excitation has long been thought to drive epileptic seizures,[3] while recent cell-specific studies have suggested a role for inhibitory neurons in both seizure initiation[6,7] and termination.[12,14] Our finding adds to the modern *E*:*I* discussion by reaffirming the classic distinction between ictal initiation and propagation. Specifically, we observed a higher ratio of recruited excitatory:inhibitory cells near the seizure initiation site compared to locations that were recruited later by the same seizure. A recent study in anesthetized mice reported a similar finding: the *E*:*I* activity ratio, calculated on averaged parvalbumin-positive and non- parvalbumin interneuron activity, was higher in the initiation zone compared to propagation zones during the pre-seizure period.[16] However, the experiment involved focal injection of 4-AP, where the assumption that the injection and onset sites are superimposed may not always be correct. Our experiments circumvent this ambiguity by allowing seizures to develop spontaneously in a model that permits whole-brain imaging so that we could identify distinct initiation zones on an event-by-event basis.

Some studies in rodents[6,13] and humans[7] have reported earlier activity from inhibitory cell populations before recruitment to seizure events. We did not observe significantly different onset timing between *E* and *I* cell types. We speculate that this could be due to

differences in recording location (initiation versus propagation zones), or possibly due to variations in technique. For example, Khoshkhoo *et al.*[13] used an optogenetic kindling model and the firing rate changes between inhibitory and excitatory cells observed by Miri *et al.* were on the order of just ~2 Hz,[6] which our calcium imaging may not have been sufficiently sensitive to detect. Our findings, therefore, do not rule out the possibility of earlier inhibitory cell activation, but do support a model of ictogenesis that depends on higher-weighted excitatory cell recruitment at initiation sites.

Numerous studies have shown that surround inhibition, present outside of an ictal focus, can play a role in restraining seizures.[16,54–58] This restraining penumbra is a region characterized by massive synaptic barrages but little neuronal firing, until a temporal point at which the seizure annexes this region.[16,55,57–59] In our study using a nuclear-localized GCaMP to focus purely on somatic activity, we did not observe significant differences in *E* and *I* cell timing, but did observe that seizure initiation zones were heavily weighted towards excitation (higher *E*:*I*) while later propagation regions were weighted towards inhibition (lower *E*:*I*). In this drug-bathed model, initiation zones arise based on inherent increased *E*:*I*, whereas propagation zones transiently resist rapid spread, presumably through a mechanism based on higher relative local inhibition. Whether the propensity for initiation zone cells to lead seizure activity reflects an upregulation of excitatory drive or downregulation of inhibitory restraint in these zones will require future work combining imaging and intracellular recording[58] to simultaneously measure synaptic barrages, spiking and whole-brain activity during seizure dynamics.

Limitations

The larval zebrafish model is increasingly being employed to test pharmacological drugs and as a model organism of various neurological disorders. However, the direct correspondence of seizure mechanisms in the zebrafish and humans is difficult to determine. Thus, while our finding that seizure initiation is associated with hyperexcitation does align with many previous studies in mammals and humans, our data cannot state certainly that human seizures follow this principle. Similarly, our use of PTZ to induce seizures may also create difficulty in comparing results with human epilepsy patients whose seizures initiate spontaneously without any pharmacological induction. We note, however, that our findings using PTZ will be directly applicable to drug screening experiments, which typically use PTZ to induce seizures. Future experiments using human brain organoids may be enlightening for both of these limitations.

Finally, our data are also limited in cell-type resolution: we separated excitatory and inhibitory cell classes based on the presence of VGlut2a (also called VGlut2.1), a vesicular glutamate transporter. VGlut2b is coexpressed with VGlut2a, but it should be noted that VGlut1 cells also exist in the zebrafish brain, although to a vastly smaller degree.[25] Because we infer inhibitory cell identity by lack of VGlut2 expression, some cells marked as inhibitory in our data could be glutamatergic. However, our primary finding that *E*:*I* balance is higher at seizure initiation sites is unlikely to be affected if only a small subset of inhibitory cells were mislabelled across the brain.

Conclusion

The goal of epilepsy research is to understand how normal brain activity transitions to an ictal state and how the event spreads across adjacent normal brain regions. In our model we found that midbrain and diencephalic regions were the most common sites of seizure initiation. Further, during individual seizures we observed significantly higher *E*:*I* ratios in initiation compared with propagation zones, supporting a model of seizures in which excitatory activity overruns inhibitory restraint to initiate the seizure while distal regions remain more protected by an inhibitory veto.[55,56,59] The differential *E*:*I* balance we report across brain regions provides a framework for designing and interpreting drug screening studies. Further, our finding of hyperexcitation in initiation zones could be leveraged to perturb neural activity in a cell-specific manner to attenuate seizure initiation or even arrest ongoing seizures.

Acknowledgements

The authors thank Catherine Schevon, Michael Wenzel, Jyun-you Liou and Jonathon Victor as well as members of the Aksay and Schwartz laboratories for constructive discussions of this manuscript.

Funding

This work has been supported by a Multidisciplinary Seed Grant from Weill Cornell Medicine (TS/EA) and BRAIN R01 NS104926 (EA).

Competing interests

The authors report no competing interests.

Supplementary material

Supplementary material is available at *Brain* online.

References

1. Ayala GF, Dichter M, Gumnit RJ, Matsumoto H, Spencer WA. Genesis of epileptic interictal spikes—New knowledge of cortical feedback-systems suggests a neurophysiological explanation of brief paroxysms. *Brain Res*. 1973;52:1–17.
2. Dichter MA, Ayala GF. Cellular mechanisms of epilepsy—A status-report. *Science*. 1987;237(4811):157–164.
3. Matsumoto H, Marsan CA. Cortical cellular phenomena in experimental epilepsy—Ictal manifestations. *Exp Neurol*. 1964; 9(4):305–326.
4. Treiman DM. GABAergic mechanisms in epilepsy. *Epilepsia*. 2001;42(Suppl 3):8–12.
5. Lillis KP, Kramer MA, Mertz J, Staley KJ, White JA. Pyramidal cells accumulate chloride at seizure onset. *Neurobiol Dis*. 2012; 47(3):358–366.
6. Miri ML, Vinck M, Pant R, Cardin JA. Altered hippocampal interneuron activity precedes ictal onset. *Elife*. 2018;7:e40750.
7. Elahian B, Lado NE, Mankin E, *et al*. Low-voltage fast seizures in humans begin with increased interneuron firing. *Ann Neurol*. 2018;84(4):588–600.
8. Toyoda I, Fujita S, Thamattoor AK, Buckmaster PS. Unit activity of hippocampal interneurons before spontaneous seizures in an animal model of temporal lobe epilepsy. *J Neurosci*. 2015;35-(16):6600–6618.
9. Klaassen A, Glykys J, Maguire J, Labarca C, Mody I, Boulter J. Seizures and enhanced cortical GABAergic inhibition in two mouse models of human autosomal dominant nocturnal

frontal lobe epilepsy. *Proc Natl Acad Sci U S A*. 2006;103(50):19152–19157.
10. Yekhlef L, Breschi GL, Lagostena L, Russo G, Taverna S. Selective activation of parvalbumin- or somatostatin-expressing interneurons triggers epileptic seizurelike activity in mouse medial entorhinal cortex. *J Neurophysiol*. 2015;113(5):1616–1630.
11. Shiri Z, Manseau F, Levesque M, Williams S, Avoli M. Interneuron activity leads to initiation of low-voltage fast-onset seizures. *Ann Neurol*. 2015;77(3):541–546.
12. Călin A, Stancu M, Zagrean AM, Jefferys JGR, Ilie AS, Akerman CJ. Chemogenetic recruitment of specific interneurons suppresses seizure activity. *Front Cell Neurosci*. 2018;12:293.
13. Khoshkhoo S, Vogt D, Sohal VS. Dynamic, cell-type-specific roles for GABAergic interneurons in a mouse model of optogenetically inducible seizures. *Neuron*. 2017;93(2):291–298.
14. Krook-Magnuson E, Armstrong C, Oijala M, Soltesz I. On-demand optogenetic control of spontaneous seizures in temporal lobe epilepsy. *Nat Commun*. 2013;4:1376.
15. Magloire V, Cornford J, Lieb A, Kullmann DM, Pavlov I. KCC2 overexpression prevents the paradoxical seizure-promoting action of somatic inhibition. *Nat Commun*. 2019;10(1):1225.
16. Wenzel M, Hamm JP, Peterka DS, Yuste R. Acute focal seizures start as local synchronizations of neuronal ensembles. *J Neurosci*. 2019;39(43):8562–8575.
17. Kalueff AV, Echevarria DJ, Stewart AM. Gaining translational momentum: More zebrafish models for neuroscience research preface. *Prog Neuropsychopharmacol Biol Psychiatry*. 2014;55:1–6.
18. Howe K, Clark MD, Torroja CF, *et al*. The zebrafish reference genome sequence and its relationship to the human genome. *Nature*. 2013;496(7446):498–503.
19. Kalueff AV, Stewart AM, Gerlai R. Zebrafish as an emerging model for studying complex brain disorders. *Trends Pharmacol Sci*. 2014;35(2):63–75.
20. Steenbergen PJ, Richardson MK, Champagne DL. The use of the zebrafish model in stress research. *Prog Neuropsychopharmacol Biol Psychiatry*. 2011;35(6):1432–1451.
21. Baraban SC. A zebrafish-centric approach to antiepileptic drug development. *Dis Model Mech*. 2021;14(7):dmm049080.
22. Baraban SC, Taylor MR, Castro PA, Baier H. Pentylenetetrazole induced changes in zebrafish behavior, neural activity and c-FoS expression. *Neuroscience*. 2005;131(3):759–768.
23. Verdugo CD, Myren-Svelstad S, Aydin E, *et al*. Glia–neuron interactions underlie state transitions to generalized seizures. *Nat Commun*. 2019;10(1):3830.
24. Baraban SC, Dinday MT, Hortopan GA. Drug screening in Scn1a zebrafish mutant identifies clemizole as a potential Dravet syndrome treatment. *Nat Commun*. 2013;4:2410.
25. Higashijima S, Mandel G, Fetcho JR. Distribution of prospective glutamatergic, glycinergic, and GABAergic neurons in embryonic and larval zebrafish. *J Comp Neurol*. 2004;480(1):1–18.
26. Dunn TW, Mu Y, Narayan S, *et al*. Brain-wide mapping of neural activity controlling zebrafish exploratory locomotion. *Elife*. 2016;5:e12741.
27. Satou C, Kimura Y, Hirata H, Suster ML, Kawakami K, Higashijima S. Transgenic tools to characterize neuronal properties of discrete populations of zebrafish neurons. *Development*. 2013;140(18):3927–3931.
28. Liu J, Baraban SC. Network properties revealed during multi-scale calcium imaging of seizure activity in Zebrafish. *eNeuro*. 2019;6(1):ENEURO.0041-19.2019.
29. Pologruto TA, Sabatini BL, Svoboda K. ScanImage: Flexible software for operating laser scanning microscopes. *Biomed Eng Online*. 2003;2:13.
30. Schindelin J, Arganda-Carreras I, Frise E, *et al*. Fiji: An open-source platform for biological-image analysis. *Nat Methods*. 2012;9(7):676–682.
31. Pnevmatikakis EA, Giovannucci A. NoRMCorre: An online algorithm for piecewise rigid motion correction of calcium imaging data. *J Neurosci Methods*. 2017;291:83–94.
32. Turrini L, Fornetto C, Marchetto G, *et al*. Optical mapping of neuronal activity during seizures in zebrafish. *Sci Rep*. 2017;7(1):3025.
33. Eimon PM, Ghannad-Rezaie M, De Rienzo G, *et al*. Brain activity patterns in high-throughput electrophysiology screen predict both drug efficacies and side effects. *Nat Commun*. 2018;9(1):219.
34. Macarron R, Banks MN, Bojanic D, *et al*. Impact of high-throughput screening in biomedical research. *Nat Rev Drug Discov*. 2011;10(3):188–195.
35. Pitkanen A, Buckmaster PS, Galanopoulou AS, Moshe SL, eds. *Models of seizures and epilepsy*. 2nd ed. Academic Press; 2017:Xxv–Xxvi.
36. Cooper K, Fink M. The chemical induction of seizures in psychiatric therapy were flurothyl (indoklon) and pentylenetetrazol (metrazol) abandoned prematurely? *J Clin Psychopharmacol*. 2014;34(5):602–607.
37. de Meduna L. New methods of medical treatment of schizophrenia. *Arch Neurol Psychiatry*. 1936;35(2):361–363.
38. Friedlander WJ. Relation of metrazol eeg-convulsant threshold and alpha index. *Electroencephalogr Clin Neurophysiol*. 1962;14:751–753.
39. Rosch RE, Hunter PR, Baldeweg T, Friston KJ, Meyer MP. Calcium imaging and dynamic causal modelling reveal brain-wide changes in effective connectivity and synaptic dynamics during epileptic seizures. *PLoS Comput Biol*. 2018;14(8):e1006375.
40. Hadjiabadi D, Lovett-Barron M, Raikov IG, *et al*. Maximally selective single-cell target for circuit control in epilepsy models. *Neuron*. 2021;109(16):2556–2572.e6.
41. Hunyadi B, Siekierska A, Sourbron J, Copmans D, de Witte PAM. Automated analysis of brain activity for seizure detection in zebrafish models of epilepsy. *J Neurosci Methods*. 2017;287:13–24.
42. Li YH, Li JJ, Lu QC, Gong HQ, Liang PJ, Zhang PM. Involvement of thalamus in initiation of epileptic seizures induced by pilocarpine in mice. *Neural Plast*. 2014;2014:675128.
43. Bin Altaf MA, Yoo J. A 1.83 μJ/classification, 8-channel, patient-specific epileptic seizure classification SoC using a non-linear support vector machine. *IEEE Trans Biomed Circuits Syst*. 2016;10(1):49–60.
44. Tsau Y, Guan L, Wu JY. Initiation of spontaneous epileptiform activity in the neocortical slice. *J Neurophysiol*. 1998;80(2):978–982.
45. Pinto DJ, Patrick SL, Huang WC, Connors BW. Initiation, propagation, and termination of epileptiform activity in rodent neocortex *in vitro* involve distinct mechanisms. *J Neurosci*. 2005;25(36):8131–8140.
46. Prince DA, Connors BW. Mechanisms of epileptogenesis in cortical structures. *Ann Neurol*. 1984;16(Suppl):S59–S64.
47. Ayas ZÖ, Kotan D. A case of first epileptic seizure diagnosed with top of the basilar syndrome. *J Neurol Stroke*. 2017;7(4):00244.
48. Chiu P, Lipnowski S, Bruni J, Burnham WM. The effect of cinromide on 'kindled' seizures in the rat. *Neuropharmacology*. 1982;21(3):273–276.
49. Mader EC Jr, Losada V, Baity JC, McKinnies EM, Branch LA. Stroke-onset seizures during midbrain infarction in a patient with top of the basilar syndrome. *J Investig Med High Impact Case Rep*. 2020;8:2324709620940497.
50. Bernasconi A, Bernasconi N, Natsume J, Antel SB, Andermann F, Arnold DL. Magnetic resonance spectroscopy and imaging of

the thalamus in idiopathic generalized epilepsy. *Brain*. 2003; 126(Pt 11):2447–2454.
51. Avoli M, Gloor P. Role of the thalamus in generalized penicillin epilepsy—Observations on decorticated cats. *Exp Neurol*. 1982; 77(2):386–402.
52. Avoli M, Rogawski MA, Avanzini G. Generalized epileptic disorders: An update. *Epilepsia*. 2001;42(4):445–457.
53. Yaksi E, Jamali A, Verdugo CD, Jurisch-Yaksi N. Past, present and future of zebrafish in epilepsy research. *FEBS J*. 2021;288-(24):7243–7255.
54. Prince DA, Wilder BJ. Control mechanisms in cortical epileptogenic foci—Surround inhibition. *Arch Neurol*. 1967; 16(2):194–202.
55. Trevelyan AJ, Schevon CA. How inhibition influences seizure propagation. *Neuropharmacology*. 2013;69:45–54.
56. Trevelyan AJ, Sussillo D, Watson BO, Yuste R. Modular propagation of epileptiform activity: Evidence for an inhibitory veto in neocortex. *J Neurosci*. 2006;26(48):12447–12455.
57. Liou JY, Ma HT, Wenzel M, *et al*. Role of inhibitory control in modulating focal seizure spread. *Brain*. 2018;141(7):2083–2097.
58. Jayant K, Wenzel M, Bando Y, *et al*. Flexible nanopipettes for minimally invasive intracellular electrophysiology in vivo. *Cell Rep*. 2019;26(1):266–278.e5.
59. Schevon CA, Weiss SA, McKhann G, *et al*. Evidence of an inhibitory restraint of seizure activity in humans. *Nat Commun*. 2012;3: 1060.